A&A 425, 1153–1159 (2004)
DOI: 10.1051/0004-6361:20041297
© ESO 2004

Astronomy & Astrophysics

Dielectronic recombination data for dynamic finite-density plasmas

VIII. The nitrogen isoelectronic sequence

D. M. Mitnik[1] and N. R. Badnell[2]

[1] Departamento de Física, FCEN, Universidad de Buenos Aires, and Instituto de Astronomía y Física del Espacio (IAFE), Casilla de Correo 67, Sucursal 28, (C1428EGA) Buenos Aires, Argentina
e-mail: dmitnik@df.uba.ar
[2] Department of Physics, University of Strathclyde, Glasgow G4 0NG, UK

Received 14 May 2004 / Accepted 23 June 2004

Abstract. Dielectronic recombination data for nitrogen-like ions forming oxygen-like ions has been calculated as part of the assembly of a level-resolved dielectronic recombination database necessary for the modelling of dynamic finite-density plasmas (Badnell et al. 2003). Dielectronic recombination rate coefficients for a selection of ions from O^+ to Xe^{47+} are presented and the results discussed.

Key words. atomic data – plasmas – atomic processes

1. Introduction

Dielectronic recombination (DR) is the dominant electron-ion recombination process in many astrophysical and laboratory plasmas. It plays an important role in determining both the level populations and the ionization balance of both high- and low-temperature non-LTE plasmas over a wide range of electron densities.

Our programme to generate a reliable DR database necessary for the spectroscopic modelling of dynamic finite-density plasmas, has been described by Badnell et al. (2003). Calculations are being carried-out initially to produce DR data for the isoelectronic sequences of all first and second row elements. So far, results have been published for the lithium (Colgan et al. 2004), beryllium (Colgan et al. 2003), boron (Altun et al. 2004), carbon (Zatsarinny et al. 2004a), oxygen (Zatsarinny et al. 2003), and neon (Zatsarinny et al. 2004b) isoelectronic sequences.

In this paper, we describe calculations and present results for DR data for nitrogen-like ions forming oxygen-like ions. The present calculations generated DR data for the total and final level-resolved rate coefficients, in intermediate coupling (IC). Total rate coefficients are presented in a compact form using a simple fitting formula. Data are presented for several ions applicable to astrophysics and magnetic fusion plasmas. The large irregularity in Z-dependence of the total DR rate coefficients makes scaling inaccurate. This is particularly problematic for low temperatures, where the $\Delta n_c = 0$ core transitions are dominant. The reason for the irregular behaviour as a function of Z is due to the fact that autoionizing levels that are just above threshold for one value of Z (giving a high contribution to the DR cross section) can move just below threshold for a neighboring $Z + 1$ member of the series, becoming a bound state and thus not contributing to DR. The present data will form part of an Atomic Data and Analysis Structure dataset (the ADAS project (Summers 1999), comprising the *adf09* files for each ion, detailing the rate coefficients to each LSJ-resolved final level. These data are also made available online at the Oak Ridge Controlled Fusion Atomic Data Center (http://www-cfadc.phy.ornl.gov).

Although studies for a few elements of this sequence have been made, there are no systematically determined DR rate coefficients for the entire sequence. The first calculations of DR rate coefficients for nitrogen-like ions were carried out by Jacobs et al. (1977a) for Fe^{19+}, Jacobs et al. (1977b) for Si^{7+}, Jacobs et al. (1979) for Ne^{3+}, Mg^{5+}, and S^{9+}, and Jacobs et al. (1980) for Ca^{13+} and Ni^{21+}. These data were fitted by Mazzotta et al. (1998) with a single formula, tabulating the related coefficients. Terao et al. (1991), and Badnell (1992), calculated the DR rate coefficient for the special case of O^+. The only detailed experimental DR measurements for nitrogen-like ions are for Fe^{19+} ($\Delta n_c = 0$ core transitions). These experimental DR results, together with four different state-of-the-art theoretical calculations, were published by Savin et al. (2002). More recently, Gu (2003) has reported result for Mg^{5+}, Si^{7+}, S^{9+},

Article published by EDP Sciences and available at http://www.aanda.org or http://dx.doi.org/10.1051/0004-6361:20041297

Ar^{11+}, Ca^{13+}, Fe^{19+}, and Ni^{21+}. We will compare our results with the detailed existing data in Sect. 3.

The plan for the remainder of the paper is as follows: in Sect. 2 we give a brief description of the theory used and the details of our calculations for the nitrogen-like ions. In Sect. 3 we present the results for the total DR rate coefficient for O^+, F^{2+}, Ne^{3+}, Na^{4+}, Mg^{5+}, Al^{6+}, Si^{7+}, P^{8+}, S^{9+}, Cl^{10+}, Ar^{11+}, Ca^{13+}, Ti^{15+}, Cr^{17+}, Fe^{19+}, Ni^{21+}, Zn^{23+}, Kr^{29+}, Mo^{35+}, and Xe^{47+} nitrogen-like ions. We finish with a short summary in Sect. 4.

2. Theory

The theoretical details of our calculations have already been described in Badnell et al. (2003). Here we outline only the main points and describe the configurations included in the calculations.

The dielectronic recombination process $\alpha^{q+}_{g\to d\to f}$ can be symbolically represented by

$$X^{q+}_g + e^- \to [X^{(q-1)+}_d]^{**} \to X^{(q-1)+}_f + h\nu \qquad (1)$$

where X^{q+}_g represents a ion with charge q, initially in either the ground state or a metastable level, $[X^{(q-1)+}_d]^{**}$ is a doubly-excited level d of the ion $X^{(q-1)+}$, and $X^{(q-1)+}_f$ is the final recombining level f. The doubly-excited level consists, in general of an excited core electron and a Rydberg electron. We include all final levels f which are stable under autoionization transitions in our totals. Partial "recombination" to autoionizing final states based on parent metastables are also tabulated. They are necessary for collisional-radiative modelling using this data in order to go over to the correct Saha-Boltzmann limit at high density.

In the independent-processes and isolated resonance approximations using distorted waves (IPIRDW), the partial dielectronic recombination rate coefficient α^{q+1}_{gf} from an initial metastable level g into a final level f of an ion X^{+q} is given by

$$\alpha^{q+1}_{gf} = \left(\frac{4\pi a_0^2 I_{\rm H}}{k_{\rm B}T_{\rm e}}\right)^{3/2} \sum_d \frac{\omega_d}{2\omega_g} e^{-E_{\rm c}/k_{\rm B}T_{\rm e}} \times \frac{\sum_l A^{\rm a}_{d\to g,E_{\rm c}l} A^{\rm r}_{d\to f}}{\sum_h A^{\rm r}_{d\to h} + \sum_{m,l} A^{\rm a}_{d\to m,E_{\rm c}l}}, \qquad (2)$$

where ω_d is the statistical weight of the $(N+1)$-electron doubly-excited resonance level d, ω_g is the statistical weight of the N-electron target initial level and the autoionization ($A^{\rm a}$) and radiative ($A^{\rm r}$) rates are in inverse seconds. Here, $E_{\rm c}$ is the energy of the continuum electron (with angular momentum l), which is fixed by the position of the resonances, and $I_{\rm H}$ is the ionization potential energy of the hydrogen atom (both in the same units of energy), $k_{\rm B}$ is the Boltzman constant, $T_{\rm e}$ the electron temperature and $(4\pi a_0^2)^{3/2} = 6.6011 \times 10^{-24}$ cm^3.

The AUTOSTRUCTURE code (Badnell 1986; Badnell & Pindzola 1989; Badnell 1997) is used to calculate multi-configuration intermediate coupling energy levels, radiative rates and autoionization rates. The code can make use both of non-relativistic and semi-relativistic wavefunctions (Pindzola & Badnell 1990). The calculations have been produced in intermediate coupling (IC) approximation. As explained in Badnell et al. (2003), AUTOSTRUCTURE employs an interpolation technique which allows the calculation of very high-n orbitals. This approach avoids the extrapolation of low-n autoionization rates or, even worse, partial dielectronic recombination rate coefficients to high-n.

The "post-processing" calculations, where the data is organized for the generation of final state level-resolved and total dielectronic recombination rate coefficients, are implemented in the ADASDR code. Radiative transitions between highly-excited Rydberg states are computed hydrogenically, and added-in during the post-processing. Also, observed energies for the core and parent levels are used at this stage to ensure accurate positioning of the resonances and, hence, accurate low-temperature rate coefficients. The ADASDR code outputs directly the *adf09* file for use by ADAS.

Due to the complexity of the modelling involved in the DR calculation, we separate the calculations for different core-excitations generating different *adf09* output files. This also enables selective upgrades of the database.

We calculated DR processes from the initial $g = 2s^22p^3$ configuration, which consists of the $^4S_{3/2}$ ground level, and the $^2D_{3/2}$, $^2D_{5/2}$, and $^2P_{1/2}$ metastable levels. (These states are fully-mixed with the $2p^5$ configuration.) The g, d and f configurations included (Eq. (1)) for the calculation of the DR process for nitrogen-like ions, through the intermediate levels having $\Delta n_{\rm c} = 0$ core transitions (i.e., core transitions from $n_{\rm c} = 2$ to $n_{\rm c} = 2$ followed by a capture in a nl Rydberg orbital) are given by:

$$2s^22p^3 + e^- \to \left\{\begin{matrix} 2s^22p^3nl \\ 2s2p^4nl \\ 2p^5nl \end{matrix}\right\} \to \left\{\begin{matrix} 2s^22p^4 \\ 2s2p^5 \\ 2p^6 \end{matrix}\right\} + h\nu. \qquad (3)$$

Radiative stabilization within the $n_{\rm c} = 2$ core is also described by the presence of the middle group of configurations. Depopulation via autoionization into the continua of levels of the $2s2p^4$ and $2p^5$ configurations was also accounted for. In this case values of n from $n = 3$ to $n = 20$ were included, and l up to $l = 15$ are calculated. An approximation for the high-level values of n orbitals (Badnell et al. 2003) was used up to $n = 999$.

The calculation for the DR process through the intermediate odd levels d produced by a $\Delta n_{\rm c} = 1$ core excitation ($n_{\rm c} = 2 \to n_{\rm c} = 3$) and a capture in an $n = 3$ Rydberg orbital, included the following intermediate d configurations:

$$\left\{\begin{matrix} 2s^22p^23s3p;\ 2s^22p^23p3d \\ 2s2p^33s^2;\ 2s2p^33p^2;\ 2s2p^33d^2;\ 2s2p^33s3d \end{matrix}\right\} \qquad (4)$$

which decay, respectively, to the following f configurations:

$$\left\{\begin{matrix} 2s^22p^33p \\ 2s2p^43s;\ 2s2p^43d \end{matrix}\right\}. \qquad (5)$$

All the intermediate configuration have odd parities and therefore, the final configurations have even parities. The same case ($\Delta n_{\rm c} = 1$ captured in $n = 3$) but for the even case includes the following intermediate configurations d:

$$\left\{\begin{matrix} 2s^22p^23s^2;\ 2s^22p^23s3d;\ 2s^22p^23p^2;\ 2s^22p^23d^2 \\ 2s2p^33s3p;\ 2s2p^33p3d; \end{matrix}\right\} \qquad (6)$$

which decay, respectively to the following f final configurations:

$$\left\{\begin{matrix} 2s^2 2p^3 3s;\, 2s^2 2p^3 3d \\ 2s2p^4 3p \end{matrix}\right\}. \quad (7)$$

For the case of the $\Delta n_c = 1$ core excitations ($n_c = 2 \rightarrow n_c = 3$) with capture in an $n > 3$ Rydberg orbital, the intermediate d manifolds included are:

$$\left\{\begin{matrix} 2s^2 2p^2 3l' nl \\ 2s2p^3 3l' nl \end{matrix}\right\} \quad (8)$$

decaying, respectively to the manifolds f:

$$\left\{\begin{matrix} 2s^2 2p^3 3l';\, 2s^2 2p^3 nl \\ 2s2p^4 3l';\, 2s2p^4 nl \end{matrix}\right\}. \quad (9)$$

In these cases values of n from $n = 4$ to $n = 15$ were included, and l up to $l = 6$ are calculated. An approximation for the high-level values of n (Badnell et al. 2003) was used up to $n = 999$.

Our calculations include full configuration mixing between the complexes listed for the target and intermediate configurations. For consistency, we allow the same configuration mixing on the continuum level calculations, in order to allow the appropriate autoionization pathways of the intermediate mixed states. Prior to the final DR calculations, the ionic thresholds were shifted to the known spectroscopic values (`http://physics.nist.gov/cgi-bin/AtData/main_asd`) by a small amount – typically in the range of 1–2 eV for high Z. The calculations for Ti^{15+}, and beyond, were performed in the semirelativistic approximation for the radial wave functions, developed by Cowan & Griffin (1976) and implemented in AUTOSTRUCTURE as is explained in Pindzola & Badnell (1990). Non-relativistic radial functions were used otherwise.

3. Results

The dielectronic recombination rate coefficients for all the selected nitrogen-like ions calculated here are available online at the Oak Ridge Controlled Fusion Atomic Data Center (`http://www-cfadc.phy.ornl.gov`). The *adf09* files for each ion provide detailed LSJ-resolved final level rates in a manner useful to fusion and astrophysical modellers. The results are given for a wide range of temperatures, from $q^2(1 \times 10^1)$ K to $q^2(1 \times 10^7)$ K, where q is the residual charge of the initial ion. All our total intermediate coupling DR rate coefficients were also fitted with the formula:

$$\alpha_g = \frac{1}{T_e^{3/2}} \sum_{i=1}^{5} c_i e^{-E_i/T_e} \quad (10)$$

where T_e is the electronic temperature (in Kelvin), and the rate coefficients have units of $cm^3\ s^{-1}$. Results of the coefficients c_i and E_i for O^+, F^{2+}, Ne^{3+}, Na^{4+}, Mg^{5+}, Al^{6+}, Si^{7+}, P^{8+}, S^{9+}, Cl^{10+}, Ar^{11+}, Ca^{13+}, Ti^{15+}, Cr^{17+}, Fe^{19+}, Ni^{21+}, Zn^{23+}, Kr^{29+}, Mo^{35+}, and Xe^{47+} nitrogen-like ions, are presented in Table 1 (for $\Delta n_c = 0$ core transitions), and Table 2 (for $\Delta n_c = 1$).

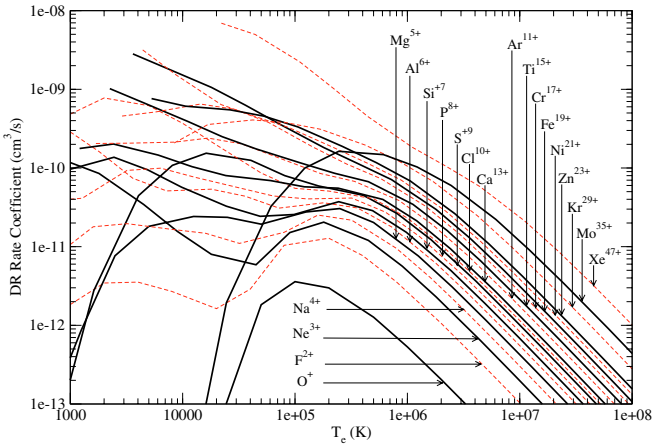

Fig. 1. Dielectronic recombination rate coefficients for O^+ to Xe^{47+} N-like ions forming O-like ions through $\Delta n_c = 0$ inner core transitions, as a function of electron temperature.

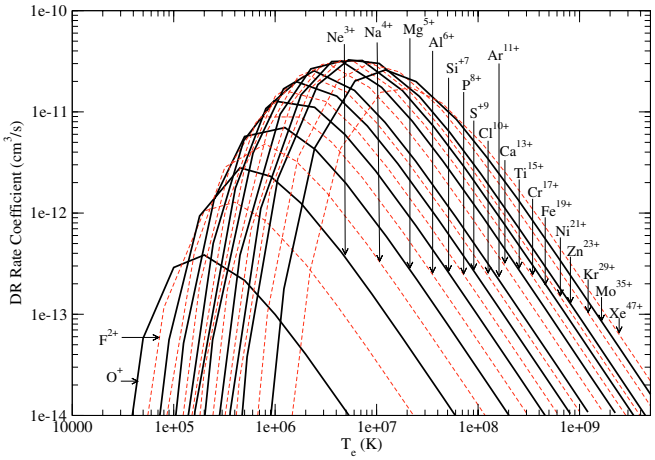

Fig. 2. Dielectronic recombination rate coefficients for O^+ to Xe^{47+} N-like ions forming O-like ions through $\Delta n_c = 1$ inner core transitions, as a function of electron temperature.

Our fits are accurate to better than 3% for all ions in the temperature range $q^2(5 \times 10^3)$ K to $q^2(1 \times 10^7)$ K.

Figure 1 shows the DR rate coefficients for O^+ to Xe^{47+} ions through $\Delta n_c = 0$ inner core transitions, as a function of electron temperature. As is shown in the figure, the DR rate coefficients behave rather irregularly at lower temperatures. Only at electron temperatures higher than $T_e = 10^6$ K is the behaviour of the DR regular, allowing for a systematic interpolation parametrization. Figure 2 shows the DR rate coefficients for O^+ to Xe^{47+} ions through $\Delta n_c = 1$ inner core transitions, as a function of electron temperature. In this case, the behaviour of the DR is regular, showing a progressive increase in the DR rate from O^+ to Xe^{47+}.

We show some separate examples of the total, $\Delta n_c = 0$ and $\Delta n_c = 1$ total DR rate coefficients from the ground state of different ions, in Figs. 3 to 7. In all cases, excepting the O^+ ion and the high-Z elements beyond Ni, we compare our data with results from the tables tabulated by Mazzotta et al. (1998). In many cases where theoretical data were not available, they use the well known Burgess General Formula (Burgess 1965).

Table 1. Fitting coefficients c_i (cm^3 s^{-1} K$^{1.5}$) and E_i (K), for Eq. (10), for DR via $\Delta n_c = 0$ core excitations, for N-like ions forming O-like ions. $X(Y)$ means $X \times 10^Y$.

Ion	c_1	c_2	c_3	c_4	c_5	E_1	E_2	E_3	E_4	E_5
O^+	1.263(−4)	1.263(−4)	1.263(−4)	1.263(−4)	1.263(−4)	1.715(+5)	1.715(+5)	1.715(+5)	1.715(+5)	1.715(+5)
F^2+	7.128(−6)	8.956(−4)	8.963(−4)	8.964(−4)	6.422(−4)	9.278(+3)	2.048(+5)	2.057(+5)	2.060(+5)	2.616(+5)
Ne^{3+}	1.364(−5)	3.784(−5)	2.040(−3)	2.237(−3)	2.097(−3)	1.270(+3)	3.053(+4)	2.401(+5)	2.408(+5)	3.018(+5)
Na^{4+}	1.431(−4)	2.151(−3)	2.522(−3)	2.522(−3)	2.522(−3)	2.488(+4)	2.589(+5)	3.134(+5)	3.134(+5)	3.134(+5)
Mg^{5+}	6.454(−5)	3.974(−4)	5.023(−3)	4.863(−3)	3.556(−3)	1.131(+4)	5.029(+4)	3.171(+5)	3.190(+5)	4.237(+5)
Al^{6+}	3.623(−5)	8.110(−4)	5.601(−3)	5.842(−3)	5.848(−3)	1.975(+3)	3.946(+4)	3.372(+5)	4.084(+5)	4.104(+5)
Si^{7+}	5.484(−5)	1.670(−4)	1.009(−3)	2.105(−2)	1.749(−4)	2.887(+3)	2.347(+4)	1.099(+5)	4.273(+5)	1.470(+6)
P^{8+}	2.462(−4)	1.802(−3)	6.819(−3)	9.331(−3)	9.330(−3)	1.004(+4)	8.336(+4)	3.967(+5)	4.993(+5)	5.008(+5)
S^{9+}	1.531(−3)	2.514(−3)	9.473(−3)	1.057(−2)	9.443(−3)	2.520(+4)	1.052(+5)	5.167(+5)	5.167(+5)	5.167(+5)
Cl^{10+}	6.761(−4)	2.269(−3)	9.156(−3)	1.305(−2)	1.308(−2)	5.502(+3)	9.248(+4)	4.138(+5)	5.987(+5)	6.035(+5)
Ar^{11+}	1.960(−4)	1.920(−3)	4.539(−3)	3.744(−2)	9.980(−5)	5.722(+3)	6.216(+4)	2.016(+5)	6.153(+5)	3.146(+7)
Ca^{13+}	2.351(−4)	2.886(−3)	6.875(−3)	2.288(−2)	2.559(−2)	5.680(+3)	3.524(+4)	1.740(+5)	6.057(+5)	7.831(+5)
Ti^{15+}	3.372(−4)	1.286(−3)	7.356(−3)	1.405(−2)	4.969(−2)	2.543(+3)	2.125(+4)	1.167(+5)	4.196(+5)	8.574(+5)
Cr^{17+}	2.305(−3)	8.774(−3)	1.406(−2)	3.658(−2)	2.933(−2)	1.303(+4)	5.568(+4)	2.853(+5)	9.206(+5)	9.206(+5)
Fe^{19+}	2.636(−7)	3.882(−3)	8.495(−3)	2.381(−2)	7.160(−2)	−2.522(+4)	8.935(+3)	6.803(+4)	3.126(+5)	1.053(+6)
Ni^{21+}	1.613(−3)	4.402(−3)	1.587(−2)	2.769(−2)	8.358(−2)	2.438(+3)	4.493(+4)	1.194(+5)	4.243(+5)	1.207(+6)
Zn^{23+}	1.258(−3)	1.196(−2)	3.141(−2)	5.950(−2)	5.330(−2)	7.705(+3)	5.639(+4)	2.391(+5)	9.261(+5)	1.572(+6)
Kr^{29+}	7.510(−3)	4.309(−2)	8.645(−2)	8.063(−2)	6.544(−2)	3.758(+4)	1.931(+5)	6.555(+5)	2.037(+6)	2.037(+6)
Mo^{35+}	2.236(−2)	1.406(−1)	1.378(−1)	1.411(−1)	7.673(−3)	2.307(+5)	6.230(+5)	2.499(+6)	2.499(+6)	8.858(+6)
Xe^{47+}	8.164(−2)	5.930(−2)	1.752(−1)	4.141(−1)	3.263(−1)	2.840(+4)	1.271(+5)	1.189(+6)	3.354(+6)	6.711(+6)

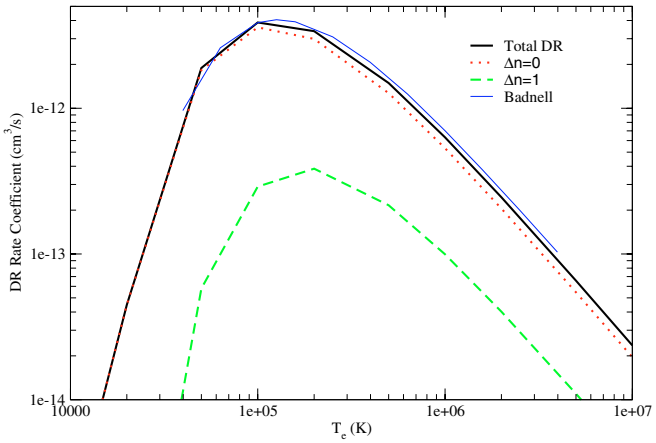

Fig. 3. Dielectronic recombination rate coefficients for O^+ forming O as a function of electron temperature. Thick solid curve: total DR, thick dotted curve: DR through $\Delta n_c = 0$ core-transitions, thick dashed curve: DR through $\Delta n_c = 1$ core-transitions. Thin solid curve: previous calculation by Badnell (1992).

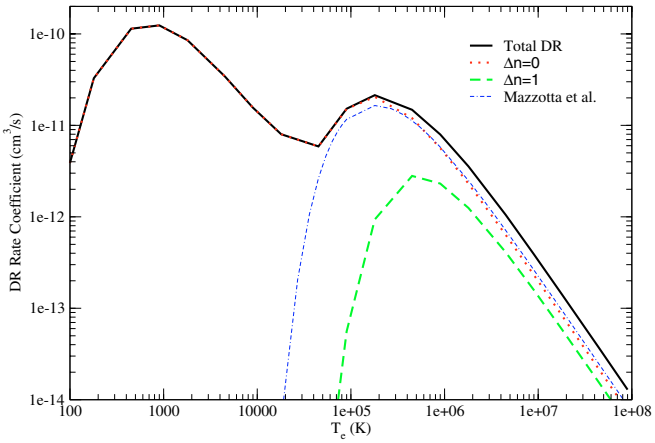

Fig. 4. Dielectronic recombination rate coefficients for Ne^{3+} forming Ne^{2+} as a function of electron temperature. Thick solid curve: total DR, thick dotted curve: DR through $\Delta n_c = 0$ core-transitions, thick dashed curve: DR through $\Delta n_c = 1$ core-transitions. Thin dotted-dashed curve: fitting formula by Mazzotta et al. (1998) to the data of Jacobs et al. (1977).

Although only designed to be used for DR via $\Delta n_c = 0$ core excitations (and H-like and H-like ions) it has been widely used outside of its range of applicability, mainly due to the lack of other data sources.

The case of O^+ can be considered a special one because, as it was pointed out by Badnell (1992), an improved atomic structure calculation is needed for accurate results. For this special case, the correlation in the N-electron configuration-interaction expansion leads to very important changes in the dominant oscillator strengths. Therefore, parametric adjusted orbitals have been used for the structure calculation, as is explained in this previous work. In Fig. 3, the intermediate coupling DR results for O^+ are also compared with the previous results obtained by Badnell (1992), showing very good agreement. These are about 25% larger than the total obtained in LS-coupling, which itself differs by less than 10% from the revised R-matrix results of Terao et al. (1991).

Table 2. Fitting coefficients c_i (cm^3 s^{-1} K$^{1.5}$) and E_i (K), for Eq. (10), for DR via $\Delta n_c = 1$ core excitations, for N-like ions forming O-like ions. $X(Y)$ means $X \times 10^Y$.

Ion	c_1	c_2	c_3	c_4	c_5	E_1	E_2	E_3	E_4	E_5
O^+	2.593(−5)	2.593(−5)	2.593(−5)	2.593(−5)	2.593(−5)	2.649(+5)	2.649(+5)	2.649(+5)	2.649(+5)	2.649(+5)
F^2+	1.018(−4)	3.461(−4)	3.461(−4)	3.402(−4)	3.977(−6)	3.790(+5)	4.970(+5)	4.970(+5)	5.573(+5)	4.773(+6)
Ne^{3+}	6.981(−5)	1.512(−3)	1.512(−3)	1.512(−3)	5.340(−5)	3.687(+5)	7.725(+5)	7.725(+5)	7.725(+5)	3.086(+6)
Na^{4+}	1.865(−3)	2.737(−3)	2.737(−3)	2.737(−3)	2.736(−3)	7.565(+5)	1.113(+6)	1.113(+6)	1.113(+6)	1.113(+6)
Mg^{5+}	2.634(−4)	8.923(−3)	8.988(−3)	8.988(−3)	1.699(−3)	5.301(+5)	1.321(+6)	1.321(+6)	1.321(+6)	2.427(+6)
Al^{6+}	1.834(−3)	1.609(−2)	1.618(−2)	1.618(−2)	4.819(−3)	8.834(+5)	1.666(+6)	1.669(+6)	1.670(+6)	2.522(+6)
Si^{7+}	3.081(−3)	3.145(−2)	3.145(−2)	3.145(−2)	1.094(−3)	9.796(+5)	2.080(+6)	2.080(+6)	2.080(+6)	6.521(+6)
P^{8+}	7.513(−3)	4.910(−2)	4.910(−2)	4.909(−2)	1.242(−3)	1.249(+6)	2.523(+6)	2.523(+6)	2.523(+6)	1.029(+7)
S^{9+}	3.353(−2)	3.865(−2)	5.576(−2)	5.616(−2)	5.577(−2)	1.938(+6)	2.447(+6)	3.256(+6)	3.272(+6)	3.279(+6)
Cl^{10+}	2.363(−2)	1.184(−1)	1.185(−1)	8.482(−2)	1.393(−3)	1.792(+6)	3.279(+6)	3.297(+6)	4.113(+6)	9.904(+8)
Ar^{11+}	4.753(−2)	1.022(−1)	1.021(−1)	1.021(−1)	1.021(−1)	2.137(+6)	4.056(+6)	4.056(+6)	4.056(+6)	4.056(+6)
Ca^{13+}	9.880(−2)	1.649(−1)	1.697(−1)	1.738(−1)	1.612(−1)	2.707(+6)	5.283(+6)	5.283(+6)	5.283(+6)	5.283(+6)
Ti^{15+}	2.271(−1)	2.261(−1)	2.261(−1)	2.261(−1)	2.261(−1)	3.599(+6)	6.795(+6)	6.795(+6)	6.795(+6)	6.795(+6)
Cr^{17+}	2.711(−1)	3.156(−1)	3.156(−1)	3.156(−1)	3.156(−1)	4.036(+6)	8.074(+6)	8.074(+6)	8.074(+6)	8.074(+6)
Fe^{19+}	1.914(−1)	5.129(−1)	5.150(−1)	4.206(−1)	3.592(−1)	3.983(+6)	7.902(+6)	7.902(+6)	1.101(+7)	1.101(+7)
Ni^{21+}	4.064(−1)	5.198(−1)	5.199(−1)	5.199(−1)	5.199(−1)	5.003(+6)	1.111(+7)	1.111(+7)	1.111(+7)	1.111(+7)
Zn^{23+}	2.659(−1)	9.651(−1)	5.184(−1)	6.934(−1)	5.438(−1)	5.058(+6)	8.946(+6)	1.426(+7)	1.426(+7)	1.426(+7)
Kr^{29+}	9.621(−1)	8.648(−1)	8.648(−1)	8.648(−1)	8.648(−1)	8.056(+6)	1.898(+7)	1.898(+7)	1.898(+7)	1.898(+7)
Mo^{35+}	8.149(−1)	9.112(−1)	1.321(+0)	1.626(+0)	1.100(+0)	1.051(+7)	1.286(+7)	2.695(+7)	2.696(+7)	2.700(+7)
Xe^{47+}	7.620(−1)	1.531(+0)	1.767(+0)	1.607(+0)	2.112(+0)	1.782(+7)	1.787(+7)	3.899(+7)	3.899(+7)	5.213(+7)

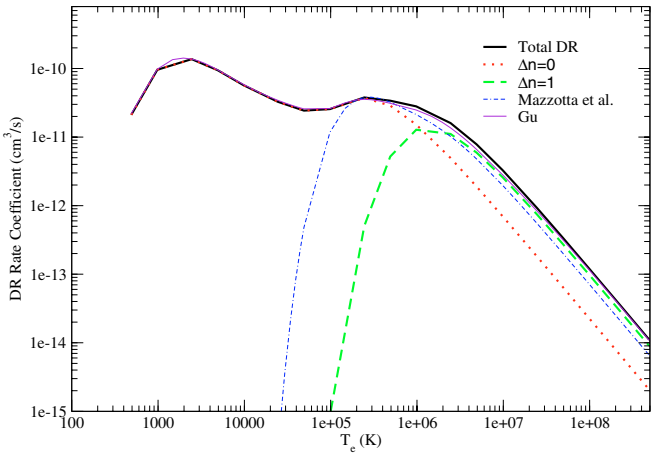

Fig. 5. Dielectronic recombination rate coefficients for Si^{7+} forming Si^{6+} as a function of electron temperature. Thick solid curve: total DR, thick dotted curve: DR through $\Delta n_c = 0$ core-transitions, thick dashed curve: DR through $\Delta n_c = 1$ core-transitions. Thin dotted-dashed curve: fitting formula by Mazzotta et al. (1998) to the data of Jacobs et al. (1977a). Thin solid curve: calculations by Gu (2003).

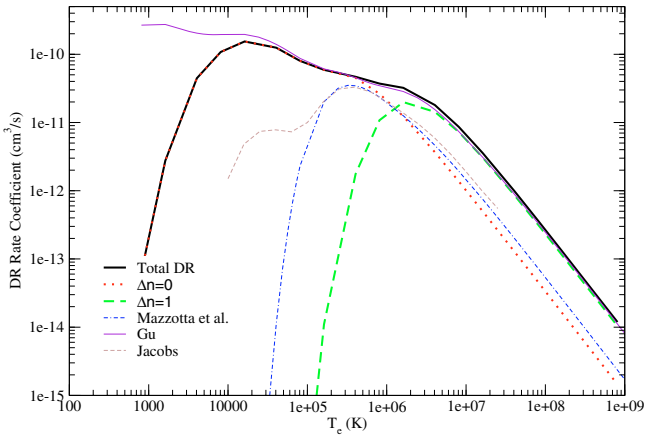

Fig. 6. Dielectronic recombination rate coefficients for S^{9+} forming S^{8+} as a function of electron temperature. Thick solid curve: total DR, thick dotted curve: DR through $\Delta n_c = 0$ core-transitions, thick dashed curve: DR through $\Delta n_c = 1$ core-transitions. Thin dotted-dashed curve: fitting formula by Mazzotta et al. (1998). Thin solid curve: calculations by Gu (2003). Thin dashed curve: calculations by Jacobs et al. (1979).

In Fig. 4 for Ne^{3+} we see the large low-temperature enhancement of the rate coefficient due to DR via low-lying resonances, typical of the $\Delta n_c = 0$ core excitation. This is not described by the data of Jacobs et al. (1979), which was fitted by Mazzotta et al. (1998). This is of relevance for the modelling of photoionized plasmas, but not collision dominated plasmas. We see a similar trend for Si^{7+} in Fig. 5, with the low temperature enhancement in close agreement with that described by Gu (2003).

The parametric data given by Mazzotta et al. (1998) for S^{9+} (Fig. 6) is the result of fitting the data calculated by Jacobs et al. (1979), which covers the electron temperature range between 10^4 K to 10^7 K. Since the fitting formula does not represent well the data of Jacobs et al., we show also the original results together with those of the fitting formula. Below

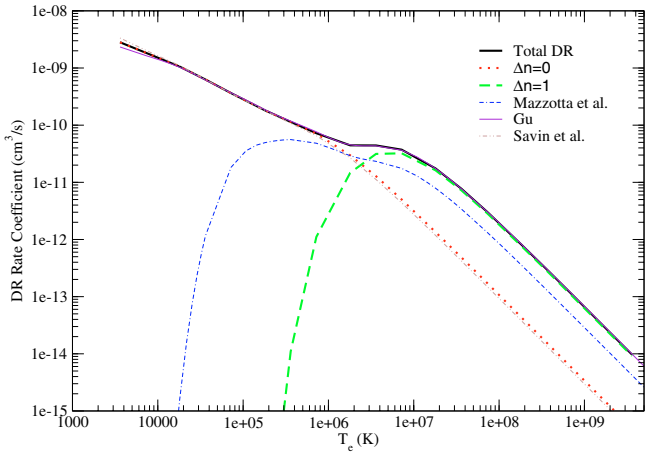

Fig. 7. Dielectronic recombination rate coefficients for Fe^{19+} forming Fe^{18+} as a function of electron temperature. Thick solid curve: total DR, thick dotted curve: DR through $\Delta n_c = 0$ core-transitions, thick dashed curve: DR through $\Delta n_c = 1$ core-transitions. Thin dotted-dashed curve: fitting formula by Mazzotta et al. (1998), based on unpublished data of Roszman. Thin solid curve: calculations by Gu (2003). Thin dotted curve: experimental results by Savin et al. (2002).

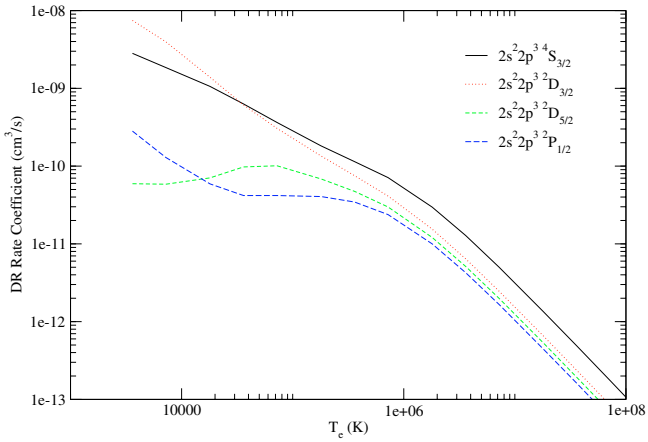

Fig. 8. Dielectronic recombination rate coefficients for Fe^{19+} forming Fe^{18+} through $\Delta n_c = 0$ core transitions, as a function of electron temperature. The different curves show the initial-state level-resolved total DR rate coefficients for the different initial metastable levels as indicated.

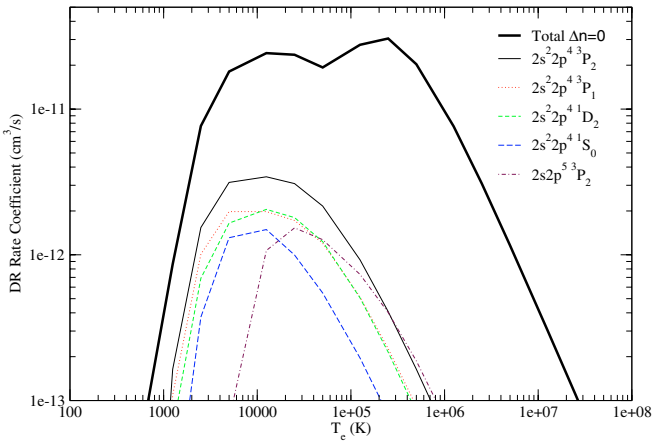

Fig. 9. Dielectronic recombination rate coefficients for Mg^{5+} forming Mg^{4+} through $\Delta n_c = 0$ core transitions, as a function of electron temperature. The different curves show final-state level-resolved rate coefficients from the initial $2s^22p^3\ ^4S_{3/2}$ level to the final levels as indicated.

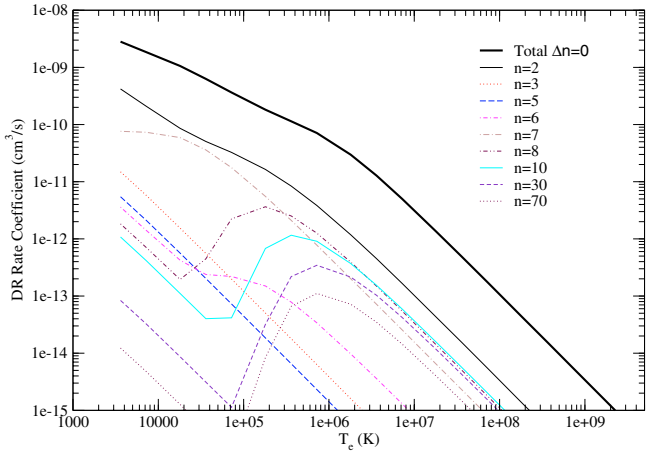

Fig. 10. Dielectronic recombination rate coefficients for Fe^{19+} forming Fe^{18+} through $\Delta n_c = 0$ core transitions, as a function of electron temperature. The different curves show the DR final-state level-resolved rate coefficients from the initial $2s^22p^3\ ^4S_{3/2}$ level to the final $2s^22p^3nl$ levels with given n.

2×10^4 K our results start fall away from those of Gu (2003). At these temperatures the DR rate coefficient is sensitive to small differences in the position of near-threshold resonances. The abundance of S^{9+} in a photoionized plasma is sharply peaked at about 3×10^4 K (Kallman & Bautista 2001). At 2×10^4 K its abundance has fallen by a factor of 10 and S^{6+} and S^{7+} are the dominant ionization stages.

In Fig. 7, the $\Delta n_c = 0$ DR results for Fe^{19+} are also compared with the experimental results obtained by Savin et al. (2002), showing an excellent agreement for a very wide range of temperatures. The parametric data given by Mazzotta et al. (1998) is based ultimately on unpublished data from Roszman which, again, does not describe the low temperature regime.

In general, DR from initial metastable levels is also required for collisional-radiative modelling of dynamic plasmas. The reason for this is that significant populations can build up in the metastables and they are not necessarily in quasi-static equilibrium with the ground state. An example of our initial level-resolved data is given in Fig. 8, where DR rate coefficients for Fe^{19+} (through $\Delta n_c = 0$ core transitions) are displayed. The figure shows DR from the initial ground $2s^22p^3\ ^4S_{3/2}$ and metastables $^2D_{3/2}$, $^2D_{5/2}$, and $^2P_{1/2}$. We show only the $\Delta n_c = 0$ contribution, because the $\Delta n_c = 1$ contribution (important only at high temperatures) is roughly the same from all the initial metastable levels. On the other hand, the $\Delta n_c = 0$ contributions from each different initial levels are quite different at low temperatures.

As an example of the final-state level-resolved rate coefficients available, we present in Fig. 9 DR rate coefficients for Mg^{5+} from the initial $2s^22p^3\ ^4S_{3/2}$ level to the final $2s^22p^4$ ($^3P_2$,$^3P_1$,$^1D_2$,$^1S_0$), and $2s2p^5\ ^3P_2$ levels. These are the

dominant path contributions (among thousand of levels) to the total DR through $\Delta n_c = 0$ core transitions.

In addition to the total DR rate coefficients, the *adf09* files also contain information about the population from DR of the resolved final levels, bundled for different *nl* manifolds, which is required for collisional-radiative modelling of dense plasmas. As an example of the final bundled n rate coefficients available, we present in Fig. 10 the $\Delta n_c = 0$ DR rate coefficients for Fe^{19+}, for population of the final $2s^2 2p^3 nl$ levels, with given n quantum numbers. As is expected, the ion preferentially recombines to the $2s^2 2p^4$ levels ($n = 2$), and in general, the contributions for the different n manifolds smoothly decrease as n increases, until a new autoionization channel is opened. For this particular case, an $n = 7$ resonant lying close to threshold produces a very large contribution at low temperatures.

4. Summary

In this paper we have described calculations of dielectronic recombination data for the nitrogen-like isoelectronic sequence forming oxygen-like ions as part of an assembly of a dielectronic recombination database necessary for the modelling of dynamic finite-density plasmas (Badnell et al. 2003). We have calculated LSJ final-state level-resolved dielectronic recombination rate coefficients in a form which will prove of great use to astrophysical and fusion plasma modellers. We have calculated data over a wide temperature range and for a large number of atomic ions in order to maximise the available information for modelling work. In order to facilitate the further application of our data, we fitted the total DR results with a standart approximation formula. Our fits are accurate to better than 3% for all ions in the temperature range $q^2(5\times10^3)$ K to $q^2(1\times10^7)$ K, where q is the residual charge of the initial ion. Comparisons have been made with the fitting formulae of Mazzotta et al. (1998), showing that their approximation is not good for the low temperature range. We found very good agreement with the results calculated by Gu (2003), and for the only detailed experimental data, Fe^{19+}, by Savin et al. (2002).

References

Altun, Z., Yumak, A., Badnell, N. R., Colgan, J., & Pindzola, M. S. 2004, A&A, accepted for publication (Paper VI)

Badnell, N. R. 1986, J. Phys. B, 19, 3827

Badnell, N. R. 1992, Phys. Rev. A, 46, 660

Badnell, N. R. 1997, J. Phys. B, 30, 1

Badnell, N. R., & Pindzola, M. S. 1989, Phys. Rev. A, 39, 1685

Badnell, N. R., O'Mullane, M., Summers, H. P., et al. 2003, A&A, 406, 1151 (Paper I of this series)

Burgess, A. 1965, ApJ, 141, 1588

Colgan, J., Pindzola, M. S., Whiteford, A. D., & Badnell, N. R. 2003, A&A, 412, 597 (Paper III)

Colgan, J., Pindzola, M. S., & Badnell, N. R. 2004, A&A, 417, 1183 (Paper V)

Cowan, R. D., & Griffin, D. C. 1976, J. Opt. Soc. Am., 66, 1010

Gu, M. F. 2003, ApJ, 590, 1131

Jacobs, V. L., Davis, J., Kepple, P. C., & Blaha, M. 1977a, ApJ, 211, 605

Jacobs, V. L., Davis, J., Kepple, P. C., & Blaha, M. 1977b, ApJ, 215, 690

Jacobs, V. L., Davis, J., Rogerson, J. E., & Blaha, M. 1979, ApJ, 230, 627

Jacobs, V. L., Davis, J., Rogerson, J. E., et al. 1980, ApJ, 239, 1119

Kallman, T., & Bautista, M. 2001, ApJS, 133, 221

Mazzotta, P., Mazzitelli, G., Colafrancesco, S., & Vittorio, N. 1998, A&AS, 133, 403

Pindzola, M. S., & Badnell, N. R. 1990, Phys. Rev. A, 42, 6526

Savin, D. W., Behar, E., Kahn, S. M., et al. 2002, ApJS, 138, 337

Summers, H. P. 1999, ADAS User Manual (2nd edition), `http://adas.phys.strath.ac.uk/adas/docs/manual`

Terao, M., Bell, K. L., Burke, P. G., & Hibbert, A. 1991, J. Phys. B, 24, L321 (Their unpublished revised results (private communication) are about 20% larger, it is these with which we compare)

Zatsarinny, O., Gorczyca, T. W., Korista, K. T., Badnell, N. R., & Savin, D. W. 2003, A&A, 412, 587 (Paper II)

Zatsarinny, O., Gorczyca, T. W., Korista, K. T., Badnell, N. R., & Savin, D. W. 2004a, A&A, 417, 1173 (Paper IV)

Zatsarinny, O., Gorczyca, T. W., Korista, K. T., Badnell, N. R., & Savin, D. W. 2004b, A&A, accepted (Paper VII)